Acoustic VTI Full-waveform Inversion with 3-D Free-surface Topography

Huiskes, M.J.; Plessix, RE; Mulder, Wim

DOI
10.3997/2214-4609.201700503

Publication date
2017

Document Version
Accepted author manuscript

Published in
79th EAGE Conference & Exhibition 2017

Th A3 01

Acoustic VTI Full-waveform Inversion with 3-D Free-surface Topography

M.J. Huiskes* (Shell Global Solutions International), R.-É. Plessix (Shell Global Solutions International), W.A. Mulder (Shell GSI BV and Delft University of Technology)

Summary

In land applications, topography may impact the imaging if not taken into account. With low-frequency and wide-aperture data, the

long-to-intermediate wavelength components of the velocity model can be

recovered by full-waveform inversion. Standard static corrections to handle

the topography do not work satisfactorily on long-offset data. We present a

method to handle 3-D free-surface topography for acoustic FWI by directly

modelling the effect of the topography with an immersed-boundary

finite-difference scheme. The numerical scheme is aimed specifically at

first-order wave equations discretized on standard staggered grids, using

high-order derivative operators that are modified based on their relative position to the free surface. We extend the approach to VTI media to be able to model velocity anisotropy required in long-offset inversions. We then investigate the topography artefacts seen on real land full-waveform inversions in relatively simple synthetic experiments, allowing us to quantify the effect of elevation variation on the inversion accuracy. The experiments demonstrate that elevation variations in the order of 1/4 wavelength or somewhat smaller can already create artefacts in the inversion results if ignored.

Introduction

In land applications, topography variation may impact the imaging if not taken into account. With low-frequency and wide-aperture data, the long-to-intermediate wavelength components of the velocity model can be recovered by full-waveform inversion. Standard static corrections to handle the topography do not work satisfactorily on long-offset data.

We present a method to handle 3-D free-surface topography for acoustic FWI by directly modelling the effect of the topography with a finite-difference scheme for the first-order wave equation introduced earlier (Huiskes et al., 2016; Mulder and Huiskes, 2017).

The method is based on an immersed interface approach (Lombard et al., 2008) in which the free surface does not have to coincide with the discretization grid, avoiding a staircase-like representation of the topography (Bohlen and Saenger, 2006). We refer to Huiskes et al. (2016) for a more detailed overview of methods for simulating seismic waves interacting with free-surface topography.

First, we review the main elements of the numerical scheme that is designed specifically for discretization on standard staggered grids (SSG) using high-order derivative operators, which are modified based on their relative position to the free surface. Next, we extend the approach to vertical transverse isotropic (VTI) media to be able to model velocity anisotropy required in long-offset inversions. In relatively simple synthetic experiments, we then reproduce topography artefacts we have seen on real land full-waveform inversions, allowing us to quantify the effect of elevation variation on the inversion accuracy.

Method

We consider the 3-D acoustic wave equation in a stress-velocity formulation. For the sake of exposition, we first consider the 2-D isotropic case. The extension to VTI will be discussed in the next section.

$$\partial_t p = -V_p^2 \rho (\partial_x v_x + \partial_z v_z), \quad \rho\, \partial_t v_x = -\partial_x p, \quad \rho\, \partial_t v_z = -\partial_z p. \tag{1}$$

Here, $p(t,x,z)$ is pressure as a function of time t and position (x,z), $v_x(t,x,z)$ and $v_z(t,x,z)$ are the horizontal and vertical velocity, respectively, $\rho(x,z)$ is the density, and $V_p(x,z)$ the P-wave sound speed. At the free-surface boundary, $\Gamma : (x(\tau), z(\tau))$, the usual zero traction condition reduces to zero pressure, $p(x(\tau), z(\tau), t) = 0$, in the acoustic case. We discretize (1) on a standard staggered grid. The free surface does not have to coincide with the discretization grid.

We use an immersed-boundary approach to formulate a finite-difference scheme for approximating spatial derivatives in (1) at grid points near the free surface. The main idea is to extend the wavefield beyond the free surface such that we can still use regular high-order derivative stencils for the derivative approximation. In our approach, we restrict ourselves to constructing 1-D extensions of the wavefield, i.e., the extended or virtual wavefield is only constructed in the direction where we need the spatial derivative. This is achieved by combining the free-surface conditions with interpolation through a number of known interior values. As we consider only 1-D extensions, an exterior grid point can sometimes be assigned several 'virtual' values if that point is required for derivatives in different directions. Figure 1 illustrates the approximation procedure.

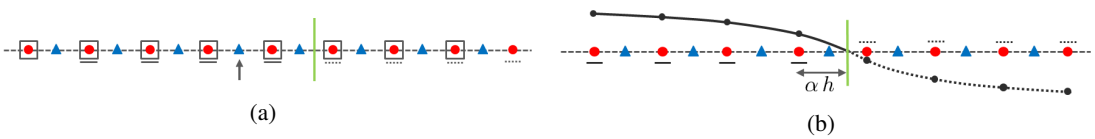

Figure 1 *(a) Pressure (●) derivative approximation at a particle velocity (▲) grid point (↑) using a regular (8-th order) derivative stencil extended beyond the free surface using field values (indicated by the squares) on both sides of the free surface (green line). (b) Pressure field extension by 1-D Taylor expansion at the free surface from interior field values (solid) to virtual field values (dashed).*

To construct the 1-D extension for an even approximation order $M = 2K$, the wavefield is represented by an M-th order Taylor expansion at the crossing of the coordinate line for the required spatial derivative and the free surface. By assuming a 1-D wave equation in that direction, the constraints on the time

derivatives of the pressure — all derivatives zero on the free surface — can be transformed into conditions on the spatial derivatives of the Taylor expansion. If we make additional assumptions of mild curvature and local invariance of the earth attributes near the free surface, it follows that all even derivatives of the pressure field and all odd derivatives of the particle velocities are zero, i.e., pressure fields must be mirrored anti-symmetrically and velocity fields symmetrically. For general 3-D topography, the resulting extension is strictly valid only in the direction normal to the free surface. Applying this extension along the coordinate directions introduces an additional numerical error, although the zero-pressure condition at the free surface is always respected. The mechanics of the field extension procedure are described in Huiskes et al. (2016). The extension scheme depends on α, the relative distance, in terms of grid cell size h, of the first interior grid point to the free surface. To obtain a stable scheme, pressure extensions for configurations with $\alpha < \frac{1}{2}$ are based on a modified scheme where the pressure value at the grid point nearest to the free surface is ignored and, instead, a pressure value one spacing further into the interior is used. The grid point nearest to the free surface is assigned a virtual value just as the external grid points. For horizontal derivatives, the field may have to be extended in two directions. We refer to Mulder and Huiskes (2017) for further details.

In our implementation, the sequence of field approximation and extension, followed by application of the derivative operator with a regular stencil, is represented by a single derivative operator with a modified stencil. The coefficients corresponding to the virtual grid points are set to zero, and the contributions of the associated virtual field values are incorporated by modifying the coefficients of the interior field values. For the source injection and receiver measurements, we also obtain modified sampling operators that are equivalent to the application of a regular sampling stencil on an extended field. The construction is based on a similar approach as for the spatial derivative operators. The adjoint scheme is similar to the forward scheme. Since the derivative operators are no longer anti-symmetric, the modified stencils must be transposed explicitly. The same holds for the reconstruction and sampling operators for source and receivers that are positioned near the free surface. The stencil modifications do not depend on the velocity model.

3-D topography for VTI media

We now consider (1) for 3-D VTI media using the formulation of Plessix and Cao (2011). Again we list the 2-D equations

$$\rho\,\partial_t v_x = -\partial_x p_h, \quad \rho\,\partial_t v_z = -\partial_z p_v, \quad \partial_t p_h = -\kappa_n(a_\eta\,\partial_x v_x + a_\delta\,\partial_z v_z),\ \partial_t p_v = -\kappa_n a_\delta(\partial_x v_x + a_\delta\,\partial_z v_z), \quad (2)$$

using $\kappa_n = \rho V_n^2$, $a_\eta = 1+2\eta$ and $a_\delta = 1/\sqrt{1+2\delta}$, where V_n, δ, η parameterize the anisotropic sound velocity (Alkhalifah et al., 2001), and p_h and p_v are the horizontal and vertical pressure.

At the free-surface boundary, $\Gamma : (x(\tau), z(\tau))$, the zero traction condition reduces to $p_v(x(\tau), z(\tau), t) = 0$. For a flat horizontal earth model, sufficient accuracy can be obtained by a mirroring approach where the pressure fields are mirrored anti-symmetrically, and the particle velocities symmetrically (e.g. Rodrigues and Mora, 1993). These are the same mirroring conditions we use in the topography scheme discussed above, but there for a free surface in arbitrary positions relative to the discretization grid.

For a horizontal flat topography, we can observe that due to the Neumann condition on the particle velocity fields, the mirroring scheme imposes zero pressure at the free surface on both the vertical and the horizontal pressure fields. Given that, a natural generalization of the isotropic scheme to VTI media is to apply the procedure so far used for the isotropic pressure to both the horizontal and vertical pressures.

As a first evaluation of the resulting numerical scheme, both forward and adjoint, we can do the following: (1) Take a VTI medium with a flat topography at a given dip angle and generate data using the VTI topography scheme. (2) Compare to reference data obtained by modelling a tilted TI medium (TTI). The TTI medium is obtained by rotating the VTI medium such that we obtain a horizontal free surface, resulting in a negative tilt angle equal to the dip angle of the free surface in the VTI medium. If we also rotate source and receivers in the same way, the resulting shot panels should be the same. Figure 2 shows an example test for a 30° dip angle, modelling diving waves in a VTI medium with a velocity gradient with depth of 0.6 s^{-1} and $\eta = 0.2$. Production settings were used for both the VTI and TTI simulations. Results are shown for a flat-spectrum wavelet with a maximum frequency of 7.5 Hz, run at 5 points per wavelength.

We have also confirmed that we can accurately invert for the main parameters (V_n, η, ρ) through synthetic tests similar to the experiments presented in the next section.

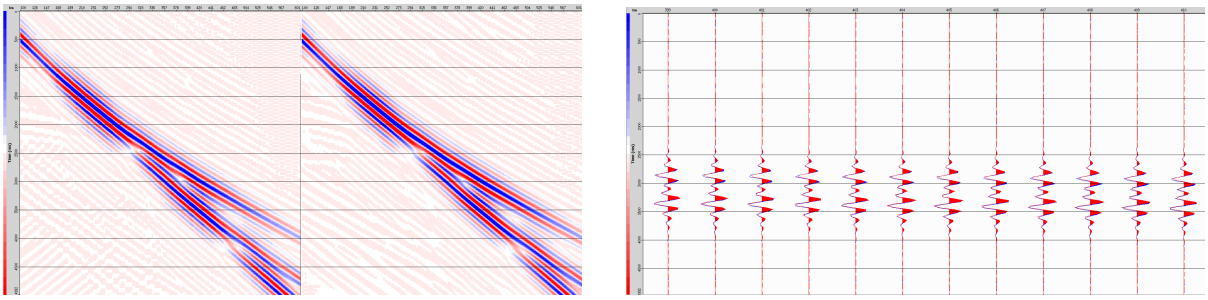

(a) (b)

Figure 2 *VTI simulation for a plane topography at 30° dip angle along the x-coordinate; source and receivers are at 15 m below the free surface, offsets up to 11 km. (a) Shot panels, left: VTI, right: TTI. (b) A zoom-in on the traces, VTI: red, TTI: blue.*

Impact of the topography on acoustic FWI

We have performed a number of synthetic experiments that demonstrate how the approach behaves under increasing elevation variation. We also assess how inversion results degrade for increasing elevation variation if the topography is not taken into account.

The approximation of topography by a horizontal free surface plane is a crude one that is nevertheless used in practice. Standard static corrections to handle the topography do not work satisfactorily on long-offset data, because they are based on near-vertical propagation. For acquisitions where the topography can be approximated by a tilted plane, we can perform the inversion in a rotated domain. Taking the topography into account by incorporating the correct 3-D free-surface boundary in the modelling has the distinct advantage that it avoids the need for cumbersome transformations and also provides more accurate results.

In the setup of Figure 3, we consider elevation undulations around a flat plane. The experiments show that we can accurately retrieve velocity anomalies for topography of varying levels of elevation variation (middle row). Also for large elevation variations the obtained update remains similar to the update obtained for a flat horizontal configuration. The velocity cross-sections on the bottom row show the effect of neglecting the elevation changes by approximating the topography by a horizontal free surface.

Elevation variations in the order of 1/4 wavelength or somewhat smaller can already create artefacts in the inversion results if ignored. For the topography with 30 m elevation variation, inversion errors are relatively mild, but at a 100 m variation, they have become significant.

Conclusion

We have presented an affordable method for handling 3-D free surface topography for isotropic and VTI acoustic FWI based on modified high-order derivative operators for first-order wave equations discretized on standard staggered grids. The results confirm that the method works for significant variation in the topography.

We have reproduced topography artefacts seen on real land full-waveform inversions through a number of synthetic experiments. The experiments demonstrate the relevance of topography inversions. In particular, we observe that elevation variations in the order of 1/4 wavelength or somewhat smaller can already create artefacts in the inversion results if ignored.

References

Alkhalifah, T., Fomel, S. and Biondi, B. [2001] The space-time domain: theory and modelling for anisotropic media. *Geophysical Journal International*, **144**(1), 105–113.

Bohlen, T. and Saenger, E.H. [2006] Accuracy of heterogeneous staggered-grid finite-difference model-

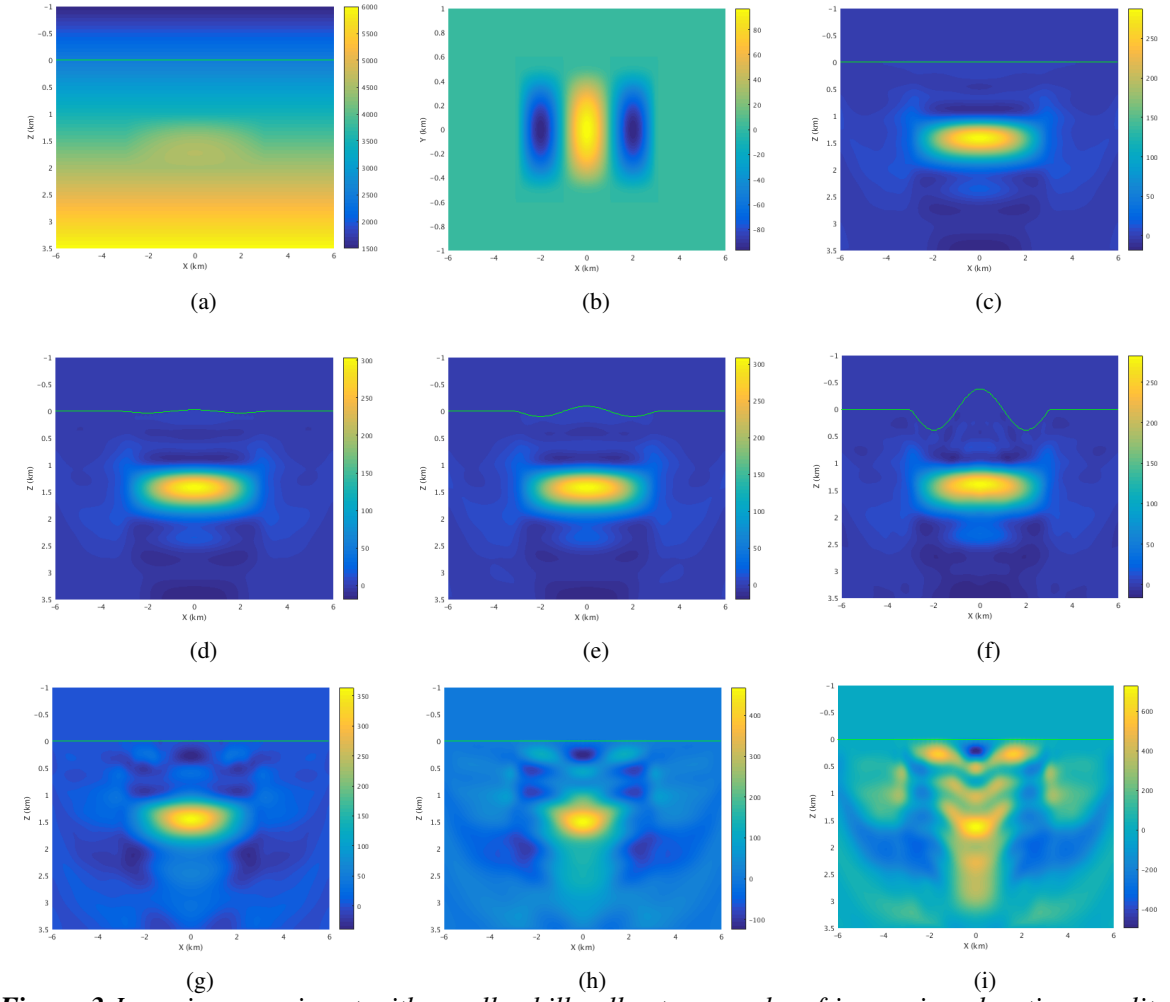

Figure 3 *Inversion experiment with a valley-hill-valley topography of increasing elevation amplitude. Inversion results shown here are after 20 iterations, based on 57 shots with a flat-spectrum wavelet with maximum frequency of 5.5 Hz. (a) True velocity model with a fast lens of maximum additional velocity of 500 m/s. (b) Valley-hill-valley topography elevation map, here with maximum elevation of 100m. (c) Inversion result obtained for synthetic data generated for a flat topography, providing a reference for the update we can expect from FWI at the current scale. (d) Inversion result obtained for a topography with elevation amplitude of 30m; the associated result obtained by neglecting this topography in the inversion is shown in (g); (e) and (h): inversion results for an elevation amplitude of 100m; (f) and (i): inversion results for an elevation amplitude of 400m.*

ing of Rayleigh waves. *Geophysics*, **71**, 109–115.

Huiskes, M.J., Plessix, R.É. and Mulder, W.A. [2016] A Fast 3-D Free-surface Topography Method for Acoustic Full-waveform Inversion. In: *78th EAGE Conference and Exhibition 2016-Workshops*.

Lombard, B., Piraux, J., Gélis, C. and Virieux, J. [2008] Free and smooth boundaries in 2-D finite-difference schemes for transient elastic waves. **172**(1), 252–261.

Mulder, W.A. and Huiskes, M.J. [2017] A simple finite-difference scheme for handling topography with the first-order wave equation. *Geophysical Journal International*, to appear.

Plessix, R.É. and Cao, Q. [2011] A parametrization study for surface seismic full waveform inversion in an acoustic vertical transversely isotropic medium. *Geophysical Journal International*, **185**(1), 539–556.

Rodrigues, D. and Mora, P. [1993] An efficient implementation of the free surface boundary condition in 2-D and 3-D elastic cases. In: *SEG Technical Program Expanded Abstracts*. 215–217.